PHYSICAL REVIEW D VOLUME 44, NUMBER 4 15 AUGUST 1991

Fractal structure in the scalar $\lambda(\phi^2-1)^2$ theory

Peter Anninos, Samuel Oliveira,* and Richard A. Matzner
Department of Physics and Center for Relativity, The University of Texas at Austin, Austin, Texas 78712
(Received 25 March 1991)

Head-on collisions of kink and antikink solitons are investigated numerically in the classical one-dimensional $\lambda(\phi^2-1)^2$ model. It is shown that whether a kink-antikink interaction settles to a bound state or a two-soliton solution depends "fractally" on the impact velocity. We discuss the results using the framework of perturbation theory which helps to clarify the nature of the fractal structure in terms of resonances with the internal shape mode oscillations. We also review the technique of collective coordinates used to reduce the infinite-dimensional system to one with just two degrees of freedom. Although we do not expect exact agreement by using such a simplification, we show that the reduced system bears a striking qualitative resemblance to the full infinite-dimensional system, reproducing the fractal structure. The maximum Lyapunov exponents are computed for the bound-state oscillations and found to be ~ 0.3 for both the full and reduced systems, demonstrating the chaotic nature of the bound state.

I. INTRODUCTION

As the Universe expands and cools, several types of topological defects can form during the spontaneous symmetry-breaking period associated with a phase transition. One such possibility is the formation of cosmic domain walls [1], which can have a number of cosmological consequences. In particular, "soft" domain walls could act as seeds for the energy-density fluctuations needed to form large-scale structure in the Universe [2]. Stebbins and Turner [3] suggest that the large-scale streaming motion observed in our local region of spacetime may be caused by a single domain wall encompassing our Hubble volume.

Domain walls can be described by a real scalar field with the $\lambda(\phi^2-1)^2$ self-interaction potential. In general, domain walls can from with all kinds of geometrical configurations. However, only the planar cosmic domain wall survives. Spherical and cylindrical walls collapse under the action of their surface tension, dissipating their energy by radiation of particles. So we expect the formation of a network of planar domain walls [4]. In this context studies of the interaction of planar domain walls among themselves are very important. It is the purpose of this paper to explore the nonlinear dynamical behavior found in the simplest of such interactions: the head-on collision of a kink and antikink pair of plane-symmetric domain walls [5]. Because the possibility of head-on collisions is small in the real Universe, our findings are not expected to have a profound effect cosmologically. However, even though our analysis is limited to one spatial dimension, we believe the results will be important in providing clues to understanding the role and behavior of more general domain-wall interactions. Also, numerous examples of kink-antikink collisions obeying similar equations of motion may be found in optics, solid-state and molecular physics, fluid dynamics, plasma, etc. [6–10]. Our results should be directly applicable to those systems as well.

The $\lambda(\phi^2-1)^2$ system is nonintegrable, contrary to its "cousin" sine-Gordon system. The kink-antikink collision in the $\lambda(\phi^2-1)^2$ system can behave both as a bion (meaning bound-) state solution or as a solution having two distinct oppositely directed solitons. Whether a kink-antikink collision settles to a bion state or a two-soliton solution depends "fractally" on the impact velocity. That is, for some velocities the interaction results in a scattering of solitons in which the kink and antikink *reflect* from each other. For other ranges of velocities, the interaction results in a bion state. In contrast, the sine-Gordon system is exactly integrable and has two-soliton and bion (breather) solutions, depending on the inverse scattering parameters. Colliding kink-antikink pairs in the sine-Gordon system pass through each other "unscathed" but for a phase shift [11].

Rarely are nonlinear dynamical systems susceptible to analytic treatment. One must often resort to perturbative or other methods to obtain a simplified system of equations to study. In this case the system with infinitely many degrees of freedom is reduced to one with just a few degrees of freedom by introducing collective coordinates [12–14] describing the gross features of the kink-antikink pair. Of course, such a reduction is justified only if the resulting equations model some features of the original system. From the mathematical point of view, it is always of interest to have one more explicit example of the treatment of an infinite-dimensional system that can be modeled by one having similarly qualitative behavior with just a few degrees of freedom.

We present an overview of the $\lambda(\phi^2-1)^2$ infinite-dimensional system in Sec. II, concentrating on the head-on collision of a kink with an antikink. We present our numerical simulations of these interactions and show the well-known two-bounce windows [13,15] in the velocity range for which the collision results in bion formation and reflection alternatively. Furthermore, we discuss an observed fractal structure showing the sequences of collision-reflection and trapped-state oscillations in the

parameter space of velocity. The perturbation theory necessary for the treatment and understanding of the kink-antikink configuration [12,13] is presented in Sec. III. In Sec. IV we review the reduction of the infinitely dimensional system to a system with just two degrees of freedom via the technique of collective coordinates and comparisons with the full infinite-dimensional system are made. It is demonstrated that although the reduced system does not represent an exact description of the infinite-dimensional system, certain features such as the fractal structure are modeled nicely by the reduced equations. Section V summarizes our conclusions.

II. COLLIDING DOMAIN WALLS

We consider the theory of a real scalar field ϕ with the scalar potential

$$V(\phi)=\frac{\lambda}{2}(\phi^2-1)^2 , \tag{2.1}$$

which has minima located at $\phi=\pm 1$ and is unbounded [$V(\phi)\rightarrow\infty$] as $\phi\rightarrow\pm\infty$. The system is defined by the Lagrangian density

$$L(x,t)=\tfrac{1}{2}\partial_\mu\phi\,\partial^\mu-\tfrac{1}{2}V(\phi) , \tag{2.2}$$

which gives, for the Euler equation of motion,

$$\frac{\partial^2\phi}{\partial t^2}-\frac{\partial^2\phi}{\partial x^2}+\lambda\phi(\phi^2-1)=0 . \tag{2.3}$$

Note that there is no reference to an expanding cosmology in Eq. (2.3). If a justification in terms of early Universe physics is required, we simply assume that the collision time scale $\approx|\phi/\dot{\phi}|$ is much smaller than the time scale of the expansion of the Universe $\approx|a/\dot{a}|$, and so we work in a Minkowski background spacetime.

Equation (2.3) has two stable vacuum solutions $\phi_\pm=\pm 1$, in addition to the topologically stable and static kink (K) solutions

$$\phi_K(x)=\tanh\left[\frac{x}{\delta}\right] , \tag{2.4}$$

where $\delta\equiv\sqrt{2/\lambda}$ is the thickness of the wall [5]. An antikink ($\bar{K}$) solution may be obtained from (2.4) by the space reflection $x\rightarrow -x$ to get $\phi_{\bar{K}}=-\phi_K$. A solution for solitons moving with speed v along the x direction is obtained by boosting the solution (2.4) to give

$$\phi_K(x,t)=\tanh\left[\frac{Z}{\delta}\right] , \tag{2.5}$$

where $Z=\gamma(x-vt)$ and γ is the Lorentz factor.

We use a numerical approach in this work to solve the dynamical equation pertaining to colliding kink-antikink pairs. The partial differential equation (2.3) is solved on a discrete spatial grid with periodic boundary conditions. Zone widths Δx in the simulations are of fixed size so the location of the nth point on the grid is given by $x_n=n\,\Delta x$. The scalar field is defined by $\phi_n(t)=\phi(x_n,t)$ for $n=1,2,\ldots,N$ on a grid with N nodes. We use a fourth-order center difference scheme to approximate the second spatial derivative [16]:

$$\frac{\partial^2\phi_n}{\partial x^2}\approx\frac{1}{12(\Delta X)^2}(-\phi_{n-2}+16\phi_{n-1}-30\phi_n+16\phi_{n+1}-\phi_{n+2})+O((\Delta x)^4) . \tag{2.6}$$

This leads to a set of N coupled second-order ordinary differential equations (ODE's) for the ϕ_n:

$$\frac{d^2\phi_n}{dt^2}=\frac{1}{12(\Delta x)^2}(-\phi_{n-2}+16\phi_{n-1}-30\phi_n+16\phi_{n+1}-\phi_{n+2})-\lambda\phi_n(\phi_n^2-1) . \tag{2.7}$$

The ordinary differential equations (2.7) are solved using a fourth-order Runge-Kutta scheme, and so our numerical algorithm is accurate to fourth order in both time and space, with errors that scale as $(\Delta t)^4$ and $(\Delta x)^4$. The accuracy of our solutions can be verified by computing the conserved energy of the system:

$$E=\int dx\left[\frac{1}{2}\left[\frac{d\phi}{dt}\right]^2+\frac{1}{2}\left[\frac{d\phi}{dx}\right]^2+\frac{\lambda}{4}(\phi^2-1)^2\right] . \tag{2.8}$$

For all cases tested, the energy was conserved to at least one part in 10^5 for the worst-case scenario simulating erratic bion states. Simulations of the less-erratic scattered two-soliton solutions preserved the energy to at least one part in 10^6.

The initial data used in our simulations represent a widely separated kink and antikink configuration moving toward each other with velocity v at $t=0$. This is accomplished through the formula

$$\phi(x,0)=\phi_K(x+x_0,0)-\phi_K(x-x_0,0)-1 , \tag{2.9}$$

and its time derivative. The expression $2x_0$ with $x_0\gg 1$ is the spatial separation of the kink centers [$\phi_K(x+x_0,0)$ is the kink solution centered at $-x_0$ and $-\phi_K(x-x_0,0)$ is the antikink at x_0]. As long as the separation distance is much larger than the thickness of the kinks ($2x_0\gg\delta$), the kink-antikink profile (2.9) is a very good approximate solution (with exponential accuracy) to the equation of motion (2.3). Note that the field takes the values $\phi(x=\pm\infty,0)=-1$ at the boundaries and $\phi(x=0,0)=+1$ at the center of mass.

Because we use periodic boundary conditions on the spatial grid, any radiation emitted during the collision process will eventually find itself back to interact with the kinks. This problem can be controlled by making the grid sufficiently large that radiation does not have time to propagate back into the grid after reaching the boundaries. It is also important that the reflected kink and antikink forms do not travel to the boundary. However, a larger grid must be discretized with a greater number of nodes for equivalent accuracy, and so we must reconcile a large grid with accuracy and computational time (N nodes imply solving $2N$ first-order ODE's). We set the left and right grid boundaries at $x_l=-40$ and $x_r=+40$. The grid is discretized with $N=1000$ nodes with zone widths $\Delta x=(x_r-x_l)/(N-1)$. The separation distance

is set by $2x_0=2[x_l+(x_r-x_l/3]$, or, equivalently, one-third of the grid length. Separation distances varied in our experiments with the larger grids used to test the effect of back radiation. All simulations presented here were run with time steps $\Delta t=0.7(\Delta x)$. The particular choices for N and Δt were experimentally determined as the least costly combination (in terms of computational time) that reproduced results from higher-resolution runs.

We now show some of the diverse output we obtained for several different incident velocities. Although radiation is very small even for the bound states and has little effect on the dynamics of the collisional process, the small dissipation of energy through radiation allows the existence of long-lived bound states. For sufficiently large velocities it is expected that the kink and antikink will reflect off each other because there is no time to radiate enough energy during the collision process to form a trapped state. This is evidenced in Fig. 1, where we display the center-of-mass evolution $\phi(x=0,t)$ for $v=0.4$. This figure clearly shows a spike representing the collision followed by a leveling off at $\phi=+1$, indicating that the kink and antikink have reflected and are receding from each other. It is also expected that for sufficiently small velocities the kink-antikink pair will have time to radiate enough of its energy to form a trapped or bion state. We demonstrate this in Fig. 2, where we plot $\phi(x=0,t)$ for $v=0.18$. The solution immediately settles to an erratically oscillating bion state.

The transition between reflection and trapped states in the parameter space of impact velocity is not a smooth one. Several authors [13,15] have reported "windows" or regions of values of v for which reflection and trapping alternate. For example, a solution representing the first window is presented in Fig. 3 for $v=0.2$ and shows the kink and antikink to collide, reflect, recede to finite separation, and then return to collide again. This state is called the two-bounce window, referring to the number of reflections. The second and third two-bounce windows are represented in Figs. 4 and 5 by $v=0.225$ and 0.238,

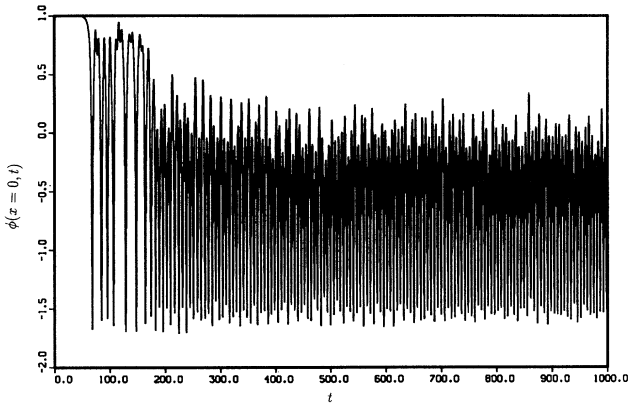

FIG. 2. Formation of a bion state with $v=0.18$ is represented by an erratically oscillating center of mass $\phi(x=0,t)$.

respectively, and differ from solutions in the first window only by a longer time interval (evidenced by additional cycle oscillations) between reflections.

Detailed information on the two-bounce windows extracted from our numerical work is presented in Table I. We have observed over 30 two-bounce windows of decreasing width in our work, but present details only for the first five in Table I, where we give the ranges of velocities ($v_1\equiv$ minimum velocity and $v_2\equiv$ maximum velocity) and the window widths ($\Delta v=v_2-v_1$). The various windows in Table I are labeled by an integer m denoting the window number. The integer m is a unique characterization of the different two-bounce windows and is related to the number of cycle oscillations (M) present between collisions (which increases by one for each higher order window as Figs. 3–5 demonstrate) by $m=M-2$. For example, in Fig. 3 we show the first two-bounce window; hence $m=1$. Also, $M=3$ since there are three cycle oscillations present (evidenced by the two large spikes and a smaller amplitude oscillation between them). We

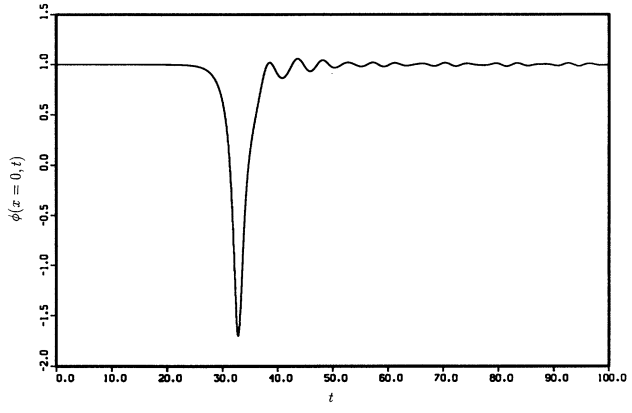

FIG. 1. Reflection of a kink and antikink is evidenced by plotting $\phi(x=0,t)$ for $v=0.4$. The collision is represented by the large spike after which kink and antikink reflect and recede from each other forming a two-soliton state.

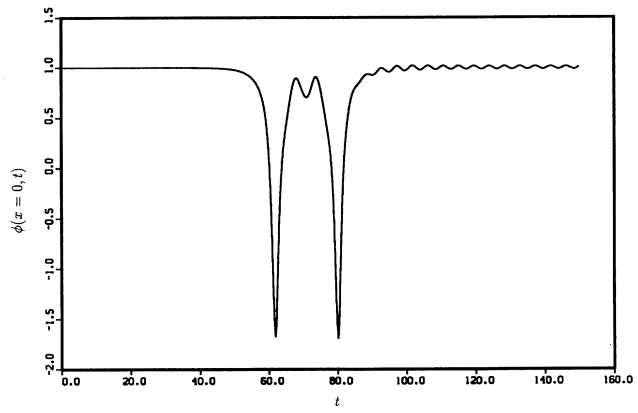

FIG. 3. First two-bounce window shown here with $v=0.2$. The kink and antikink collide, reflect, recede, and then return to collide again.

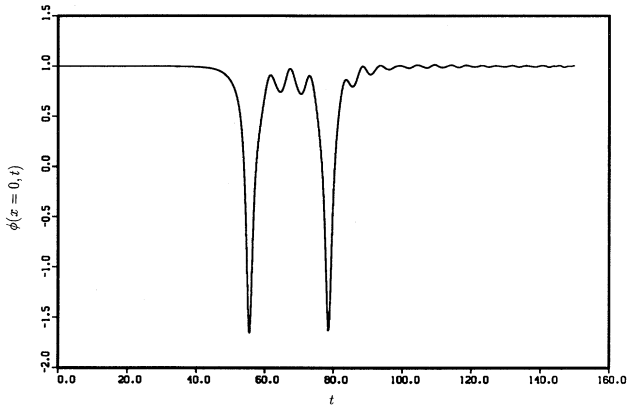

FIG. 4. Second two-bounce window shown for $v=0.225$ differs from the first two-bounce window only by a longer time interval between reflections, allowing for an additional cycle oscillation between collisions.

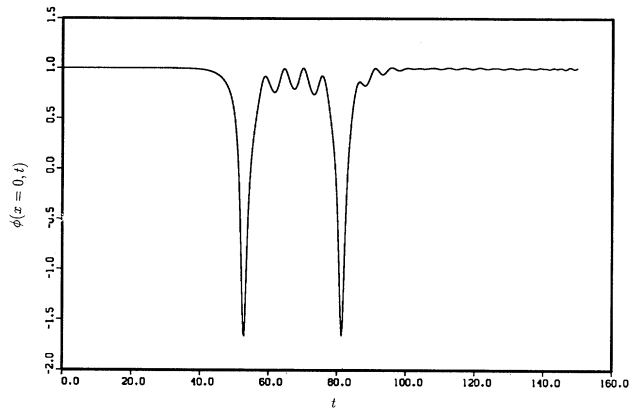

FIG. 5. Third two-bounce window shown for $v=0.238$ differs from the first and second two-bounce windows by a longer time interval between reflections allowing for an additional cycle oscillation between collisions.

also present in Table I results from an approximate scaling relation found between the different windows. In formulating this relation we assume that the window widths are inversely proportional to some power of the number of internal mode oscillations $\Delta v \propto M^{-\beta}$. Normalizing the window widths with respect to the $m=1$ window, we obtain a solution for $\beta=-\ln(\Delta v_n)/\ln(M_m/M_{m=1})$, where $\Delta v_n=\Delta v_m/\Delta v_{m=1}$. The variables Δv_n and β are presented in Table I and the constant values of β indicate the scaling relation is an accurate description.

We have found that the parameter space is much more complex than the above description because the regions between the two-bounce windows are not simple bion states. In fact, the edges of the two-bounce windows are not sharp well-defined regions. They appear to be fractal containing a hierarchial structure of n-bounce windows with $n \geq 3$ at all scales that we have observed. This is better demonstrated diagrammatically in Fig. 6. Figure 6(a) shows the two-bounce windows in dark with the rightmost dark region (beginning at $v \approx 0.25$) representing the single-bounce state above which no bion states exist and the leftmost white region (beginning at $v \approx 0.19$) representing bion states below which no reflection windows exist. In between are two-bounce windows of decreasing widths separated by regions of bion formation. If one zooms in on the edge of a typical two-bounce window (for example, the second two-bounce region outlined by a box) in Fig. 6(a), one finds what appears to be a self-similar structure [drawn in Fig. 6(b)] where now the dark regions represent three-bounce windows of decreasing widths. Zooming in once again on the outlined region of a typical three-bounce window of Fig. 6(b), one finds similar sequences of four-bounce windows [Fig. 6(c)]. The basic feature of this fractal may be described as an endless succession of higher-order n-bounce windows with decreasing widths and separations converging on the edge of a $(n-1)$-bounce window. This remarkable self-similar fractal structure was found on both edges of all n-bounce windows that we have investigated. It should be noted that Fig. 6 is only a schematic and the window structures are not drawn to scale.

We display in Figs. 7 and 8 the first two three-bounce windows with $v=0.2062$ and 0.2049, respectively, to show that they are qualitatively similar to the two bounce ones. The chosen velocities lie in three-bounce windows found on the edge of the first two-bounce window. Figures 9 ($v=0.2298$) and 10 ($v=0.229\,33$) show the first two three-bounce windows found on the edge of the second two-bounce window. From Figs. 7–10 it can be seen that the signature of the two-bounce window, in which the three-bounce solution can be found, is preserved. That is, the complete sequence of "splashes" and small cycle oscillations separating them can be used to place any n-bounce result properly in the fractal hierarchy. The first two "splashes"tell of the two-bounce window edge that harbors the sequence of three-bounce windows. The number of cycle oscillations between the second and third "splashes" then distinguishes the

TABLE I. Initial impact velocity intervals for the first five windows in the two-bounce kink-antikink interactions for the fully infinite-dimensional system.

m	v_1	v_2	Δv	Δv_1	β
1	0.192 575	0.203 425	0.010 850	1.0	
2	0.224 041	0.228 851	0.004 810	0.443 318	2.83
3	0.237 127	0.239 646	0.002 519	0.232 166	2.86
4	0.243 969	0.245 460	0.001 491	0.137 419	2.86
5	0.248 034	0.248 996	0.000 962	0.088 664	2.86

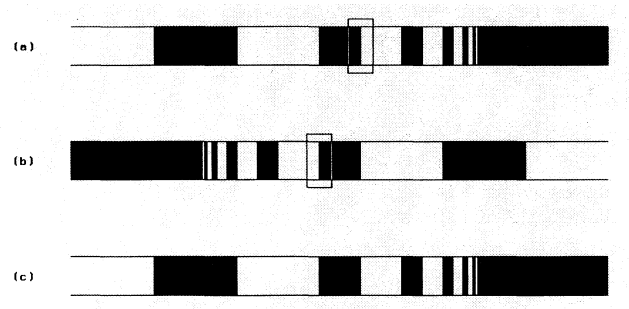

FIG. 6. Fractal structure composed of sequences of different n-bounce windows.

correct window among all those in the endless sequence of three-bounce windows.

We have summarized the properties of the first five three-bounce states near the first and second two-bounce windows in Tables II and III, respectively. We point out that because the window edges are fractal, the numbers presented in the tables can only be approximate and do not represent exact boundaries. The normalization of window widths (Δv_n) are made with respect to the same window as that in Table I, namely, the window with a single-cycle oscillation between reflections. A comparison of the normalized widths and the scaling power β in each table supports our earlier claim (made visually) that the fractal of Fig. 6 is self-similar. When rescaled to the proper window, the structure present at different scales is found to be identical both visually and quantitatively.

Finally, in this section we study the nature of the bion state formed in the space of impact velocity separating the different reflection windows. Bion states in the $\lambda(\phi^2-1)^2$ theory are more complex than the exact breather solutions of the sine-Gordon equation. Are the complex oscillations we have observed for the bion state chaotic?

To address this question we generate a time series for $\phi(0,t)$ with intervals dt between data for the bion state resulting from a $v=0.18$ collision (see Fig. 2). The time series was started after a sufficiently long time ($t=t_0\geq 200$) to eliminate transients and model only the bion-state oscillations. The time delay embedding technique is an appropriate method to reconstruct the phase space and obtain the maximum Lyapunov exponent [17,18]. Let $V(t)\equiv\phi(0,t)$. A d-dimensional vector $\mathbf{V}_i$ is constructed as

$$\mathbf{V}_i=[V_1(t_i),V_2(t_i),\ldots,V_d(t_i)]\ , \tag{2.10}$$

where d is the assumed dimension of the "attractor", $V_k(t_i)=V(t_i+(k-1)\tau)$, and τ is the time delay. Let T be the characteristic time scale for the system. For the bion we use the result from perturbation theory (discussed below in Sec. III), $T=2\pi/\omega\approx 5.1$. We made several runs with $\tau\geq T/d$.

To obtain the largest Lyapunov exponent, we choose a pair of vectors, say, $\mathbf{V}_0$ and $\mathbf{V}_0'$, such that

$$\|\mathbf{V}_0-\mathbf{V}_0'\|<\delta_0\ , \tag{2.11}$$

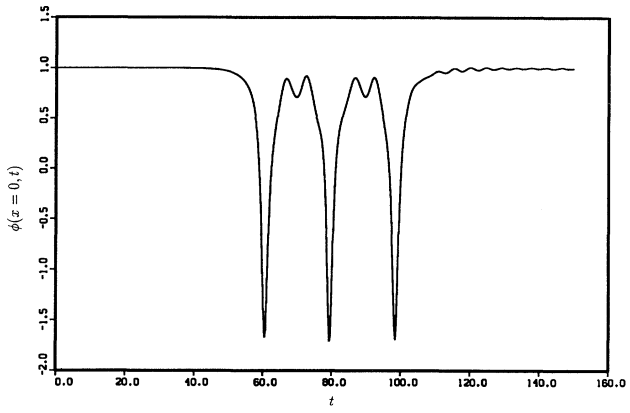

FIG. 8. Second three-bounce window ($v=0.2049$) near the first two-bounce region.

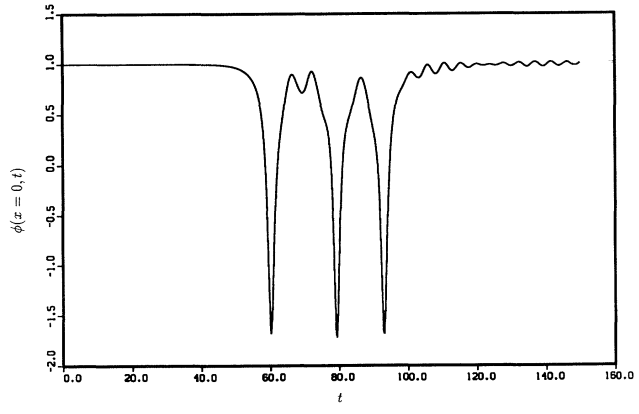

FIG. 7. First three-bounce window ($v=0.2012$) near the first two-bounce region.

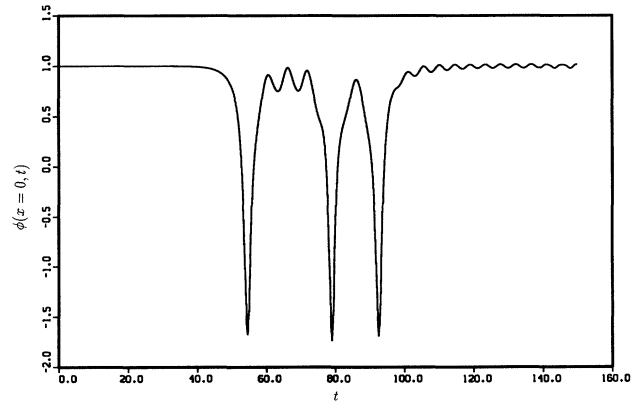

FIG. 9. First three-bounce window ($v=0.2298$) near the second two-bounce region.

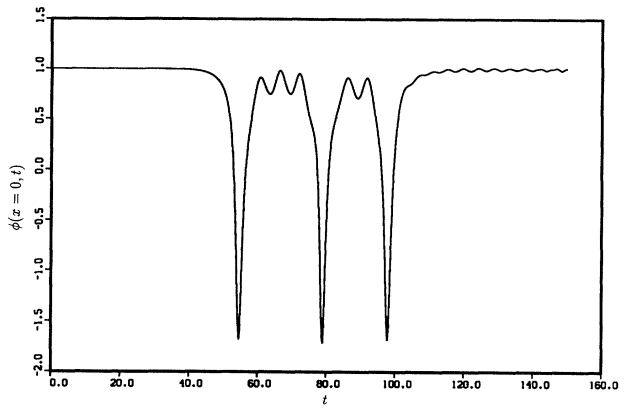

FIG. 10. Second three-bounce window ($v=0.229\,33$) near the second two-bounce window.

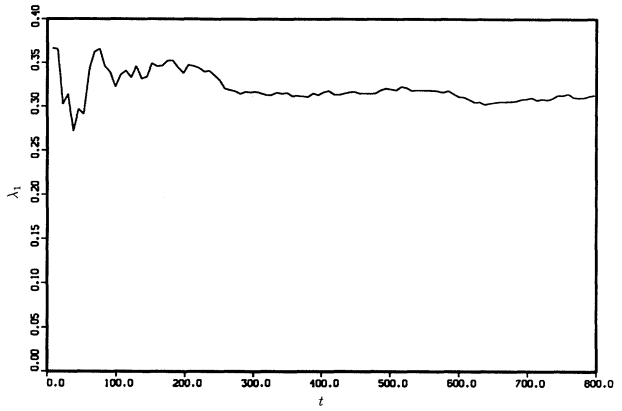

FIG. 11. Maximum Lyapunov exponent for a bion state with $v=0.18$ approaches the positive value $\lambda_1=0.31$, indicating the chaotic nature of the oscillatory trapped state.

where $||\ ||$ is the Euclidean norm and δ_0 is a small distance ($\delta_0<10^{-6}$ for all cases we tried). The quantity

$$\lambda_j=\log_2\frac{\delta_{j+1}}{\delta_j} \tag{2.12}$$

is computed for each time interval dt. If the time series represents chaotic motion, the distance between vectors grows exponentially. After a time Δt the largest Lyapunov exponent is calculated as the average of the different λ_j:

$$\lambda_1=\frac{dt}{\Delta t}\sum_j \lambda_j\ . \tag{2.13}$$

A new partner vector is then chosen using a Gram-Schmidt reorthonormalization procedure so that the two vectors are close again. Care is taken to choose a new vector with the same angular orientation as the discarded one (or at least to within a small error). The reorthonormalization time Δt is chosen to be $\Delta t \gtrsim T$.

We computed Lyapunov exponents for several different input parameters: $2<d<9$, $T/d<\tau<4T/d$, $1<\Delta t<4T$, and angular error within 10°. All results consistently give a narrow window for the value of λ_1, provided we use a sufficient number of points to construct the vectors (approximately 6000 points over the time interval of 1000 in our dimensionless units). The time evolution of a typical case is presented in Fig. 11, where the input parameters are $d=4$, $\tau=3T/8$, and $\Delta t=3T/2$. Figure 11 clearly shows that λ_1 approaches a positive constant value $\lambda_1\approx 0.31$ at $t-t_0=800$, suggesting that bion-state oscillations are chaotic.

III. PERTURBATION THEORY AND INTERNAL SHAPE-MODE OSCILLATIONS

Linear superposition of kink and antikink solutions (2.9) is not an exact solution to the nonlinear equation of motion (2.3). However, perturbation theory is extremely useful in understanding the results in the previous section and motivating what follows. In reviewing the fluctuation modes around kink and antikink solutions, we introduce $\eta(x,t)$ as a small perturbation:

$$\phi\approx\phi_K(Z)+\eta(x,t)\ . \tag{3.1}$$

Substituting this expression into the field equation (2.3) and linearizing, we get

$$\frac{\partial^2\eta}{\partial t^2}-\frac{\partial^2\eta}{\partial x^2}+\lambda\left[3\tanh^2\left[\frac{Z}{\delta}\right]-1\right]\eta=0\ , \tag{3.2}$$

for the fluctuations η around the kink and antikink. We solve for the normal modes by setting

$$\eta(x,t)=e^{i\omega t}\chi(Z)\ . \tag{3.3}$$

Substituting (3.3) into (3.2) and assuming only for $\omega\neq 0$

TABLE II. Initial impact velocity intervals for the first five windows in the three-bounce kink-antikink interactions found near the first two-bounce window. Results are for the fully infinite-dimensional system.

m	v_1	v_2	Δv	Δv_n	β
1	0.206 175 2	0.206 532 0	0.000 356 8		
2	0.204 847 4	0.205 017 5	0.000 170 1	1.0	
3	0.204 302 5	0.204 378 8	0.000 076 3	0.448 559 6	2.79
4	0.204 019 4	0.204 059 9	0.000 040 5	0.238 095 2	2.81
5	0.203 855 8	0.203 881 4	0.000 025 6	0.150 499 7	2.73

TABLE III. Initial impact velocity intervals for the first five windows in the three-bounce kink-antikink interactions found outside the second two-bounce window. Results are for the fully infinite-dimensional system.

m	v_1	v_2	Δv	Δv_n	β
1	0.229 755 7	0.229 893 7	0.000 138 0		
2	0.229 303 5	0.229 368 3	0.000 064 8	1.0	
3	0.229 127 8	0.229 158 6	0.000 030 8	0.475 308 6	2.59
4	0.229 039 5	0.229 056 3	0.000 016 8	0.259 259 2	2.64
5	0.228 989 1	0.228 999 3	0.000 010 2	0.157 407 4	2.67

that $|v|\gamma \ll |w\chi/(d\chi/dZ)|$ (that is, $\omega \gg |v|\gamma/\delta$, corresponding to a stationary limit in which the translational dynamics is dominated by the relatively high-frequency oscillations of the normal-mode vibrations), we get the eigenvalue equation

$$\left[-\frac{\partial^2}{\partial Z^2}-\frac{6}{\delta^2}\operatorname{sech}^2\left[\frac{Z}{\delta}\right]\right]\chi(Z) = \left[w^2-\frac{4}{\delta^2}\right]\chi(Z) . \quad (3.4)$$

This is the Schrödinger equation with a reflectionless potential and also the equation describing the two-soliton solution for the Korteweg–de Vries (KdV) equation [11]. The eigenvalue equation (3.4) has two discrete roots (eigenvalues) and eigenvectors given by [11,12]

$$\omega_0^2=0, \quad \chi_0(Z)=\left[\frac{3}{4\delta}\right]^{1/2}\operatorname{sech}^2\left[\frac{Z}{\delta}\right] \propto \frac{\partial}{\partial Z}\phi_K(Z) , \quad (3.5)$$

and

$$\omega_1^2=\frac{3}{\delta^2} , \quad \chi_1(Z)=\left[\frac{3}{2\delta}\right]^{1/2}\tanh\left[\frac{Z}{\delta}\right] \times\operatorname{sech}\left[\frac{Z}{\delta}\right] . \quad (3.6)$$

In addition, Eq. (3.4) has a continuous spectrum of solutions with eigenfunctions that behave as dispersive plane waves at asymptotic infinity with frequency $\omega_k^2=4/\delta^2+k^2$. The continuous spectrum is identified with a boson mode of mass $\mu=2/\delta=\sqrt{2\lambda}$.

The translational mode $\omega_0=0$ appears in virtue of the translational symmetry of one kink configuration. That is, $\chi_0(Z)$ is the infinitesimal translation correction to the kink solution. The internal shape-mode oscillations ($\omega_1=3/\delta^2=3\lambda/2$) represent localized deformations of the kink-antikink solutions. In Fig. 12 we present a superposition of the kink solution $\phi_K(x)$ in the solid line and the kink solution with perturbations due to the shape-mode eigenfunctions $\phi_K(x)\pm 0.3\chi_1(x)$ in the dotted lines.

At spatial infinity the linear superposition of one kink and one antikink is an approximate solution of the nonlinear equation of motion. As they approach each other, perturbations in each are excited by the proximity of the other. Campbell *et al.* [13] proposed that a resonance of energy exchange between the internal shape mode and the translation mode accounts for the two-bounce windows. They claim that the first reflection sets up internal shape oscillations, which take energy from the kinetic energy of the walls, resulting in binding kink with antikink. The second collision destroys the shape vibrations, putting energy back into the translational mode, unbinding the pair. Annihilation of the shape modes must coincide with some characteristic phase angle of the internal vibrations. Thus Campbell *et al.* were led to deduce that the condition for the restoration of translational or kinetic energy after the second collision should take the form

$$\omega_1 T=2\pi m+\theta , \quad (3.7)$$

where T is the time between collisions, m is an integer, and θ is a phase shift.

In Figs. 13 and 14 we plot the time between bounces versus window number for the two- and three-bounce cases, respectively. The circles in Figs. 13 and 14 represent numerical results, and the straight lines are a least-squares fit to the data. Data for the three-bounce cases presented here were taken from the vicinity of the second two-bounce window. The slopes in both Figs. 13

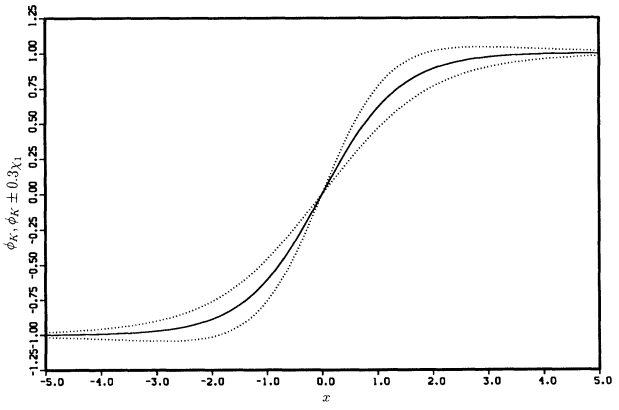

FIG. 12. Superposition of the kink solution (solid line) and the kink solution with perturbations due to the shape-mode eigenfunctions (dotted line).

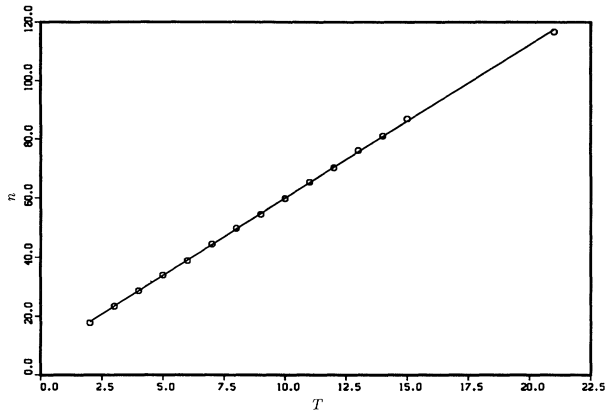

FIG. 13. Window number vs time between reflections for the two-bounce windows. Circles represent code results, and the straight line is a least-squares fit with slope 5.23.

and 14 were found from the least-squares fit to be 5.23, which compares well with the value $2\pi/\omega_1 \approx 5.13$ that one expects from (3.7). In computing these slopes we used data from the first 14 two-bounce windows (we also include the 20th window to demonstrate that this pattern continues in the same fashion for higher-order windows) and the first eight three-bounce windows. This verifies the resonance structure of the n-bounce windows as an energy exchange between translational and internal mode vibrations or, equivalently, a competition between two-soliton and bion-state solutions. Note also that Eq. (3.7) predicts that an additional cycle oscillation must occur between collisions in the mth n-bounce window compared to the $(m-1)$st n-bounce window preceding it. This is exactly what we have observed in Figs. 3–5 and 7–10.

IV. REDUCED SYSTEM

We will use collective coordinates to reduce the dynamical system (2.3) to a Hamiltonian system with just

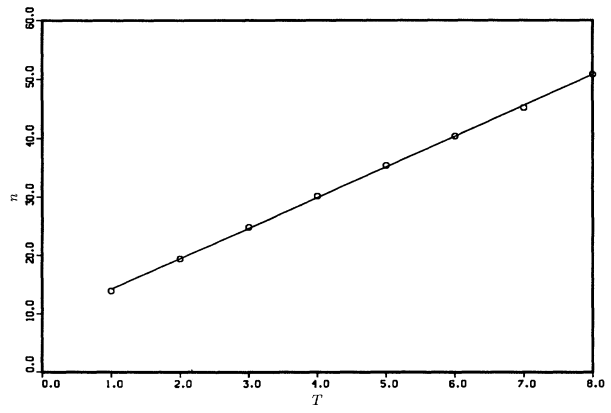

FIG. 14. Window number vs time between reflection for the first eight three-bounce windows found near the second two-bounce window. Circles represent code results, and the straight line is a least-squares fit with slope 5.23.

two degrees of freedom. In analogy with Eqs. (2.9) and (3.1) and following the work of Sugiyama [12], we assume a colliding kink-antikink system with the field configuration

$$\phi(x,t)=\phi_k(x+X(t))-\phi_K(x-X(t))-1 + A(t)[\chi_1(x+X(t))-\chi_1(x-X(t))] . \quad (4.1)$$

The variable $X(t)$ is introduced as the collective coordinate representing half the distance between the kink and antikink, $\phi_K(x)$ and $\chi_1(x)$ are given by (2.4) and (3.6), respectively, and $A(t)$ is the amplitude of the internal vibration modes. Note that $X(t)$ and $A(t)$ are related to the center-of-mass evolution $\phi(x=0,t)$ by [see Eqs. (4.1), (3.6), (2.9), and (2.5)]

$$\phi(0,t)=2\tanh\left[\frac{X(t)}{\delta}\right]-1+2A(t)\chi_1(X(t)) . \quad (4.2)$$

We define the effective Lagrangian of the finite-dimensional system as [12,15]

$$L(X,\dot{X},A,\dot{A})=\int dx\left[\tfrac{1}{2}\partial_\mu\phi\,\partial^\mu\phi-\tfrac{1}{2}V(\phi)\right] , \quad (4.3)$$

where $V(\phi)$ is the self-interacting potential given by (2.1) with $\lambda=1$. Substituting (4.1) into (4.3) gives

$$L(X,\dot{X},A,\dot{A})=[M_0+I(X)]\dot{X}^2-U(X)+\dot{A}^2 -\omega_1^2A^2+2F(X)A+2C(X)\dot{A}\dot{X} , \quad (4.4)$$

for the effective Lagrangian when the higher-order terms of A and $\dot{X}$ have been neglected on the assumption that they are small (A is the amplitude of internal mode perturbations and the impact velocity must be less than the speed of light, $|\dot{X}|\equiv|v|<1$). To help simplify the system further, we have not included terms in (4.4) that couple the $\chi_1(x+X)$ and $\chi_1(x-X)$ modes. Also, we have defined

$$\begin{aligned}
&M_0=\frac{2\sqrt{2}}{3} ,\\
&I(X)=3M_0(1-\tanh^2\alpha)(\alpha-\tanh\alpha)\coth^3\alpha ,\\
&U(X)=6M_0[-\tfrac{2}{3}+\alpha+3\coth\alpha -(2+3\alpha)\coth^2\alpha+2\alpha\coth^3\alpha] ,\\
&F(X)=\frac{3\pi}{2\sqrt{M_0}}\tanh^2\alpha(1-\tanh^2\alpha) ,\\
&C(X)=\frac{\pi}{2\sqrt{M_0}}\tanh\alpha(1-\tanh^2\alpha) ,
\end{aligned} \quad (4.5)$$

where $\alpha=\sqrt{2}X$. A comparison of the two terms $F(X)A$ and $C(X)\dot{A}\dot{X}$ shows that the assumption $v\ll\omega_1\delta^2$ justifies neglecting the $C(X)$ as a higher-order term and we do so in our analysis. This condition is appropriate in our simulations of thick domain walls. Figure 15 shows the behavior of the variables I (dashed line), U (solid line), and F (dotted line) as functions of X. Note that $U(X)$ has a shape similar to the van der Walls potential for large neutral molecules or atoms with "perfect shielding" [19].

The Lagrangian (4.4) leads us to the Hamiltonian

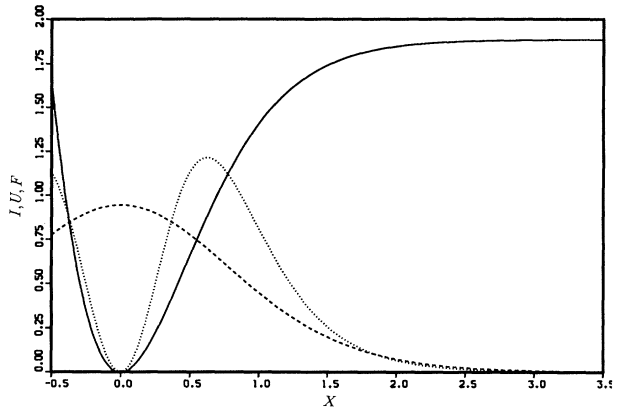

FIG. 15. Behavior of the functions I (dashed line), U (solid line), and F (dotted line) as functions of the separation distance X.

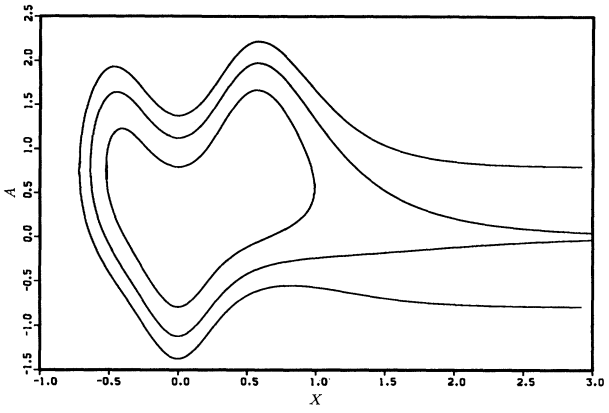

FIG. 16. Various level curves for the effective potential V_{eff} with $V_{\text{eff}}=M_0$, $2M_0$, and $3M_0$.

$$H(X,P_X,A,P_A)=\frac{P_X^2}{2D(X)}+\frac{P_A^2}{4}+U(X)+w_1^2A^2-2F(X)A\ , \tag{4.6}$$

where we have dropped the term with $C(X)$ and defined

$$P_X=D(X)\dot{X}\ ,\quad P_A=2\dot{A}\ ,\quad D(X)=2[M_0+I(X)]\ . \tag{4.7}$$

The Hamiltonian (4.6) is a more simplified version of the form found by Sugiyama [12] and is identical to the Hamiltonian used by Belova and Kudryavtsev [15] in demonstrating a qualitative likeness to the field equation (2.3). Hamilton's equations are the inverse of Eq. (4.7) together with

$$\dot{P}_X=-\frac{\partial H}{\partial X}\ ,\quad \dot{P}_A=-\frac{\partial H}{\partial A}\ . \tag{4.8}$$

Equations (4.8) are a Hamiltonian system with two degrees of freedom resulting in the following second-order differential equations:

$$\ddot{X}=\frac{1}{2(M_0+I)}(-I'\dot{X}^2+2F'A-U')\ ,\quad \ddot{A}=-\omega_1^2A+F\ , \tag{4.9}$$

where the prime is equivalent to d/dX.

The fixed points of the above set of equations are the stationary points of the effective potential

$$V_{\text{eff}}(X,A)=U(X)+\omega_1^2A^2-2F(X)A\ , \tag{4.10}$$

defined in the Hamiltonian (4.6). A linear stability analysis for perturbations near these fixed points shows that there are two elliptic points for this system: $(X_0,A_0)=(0,0)$ and $(X_2,A_2)=(0.5144,0.7671)$ with eigenvalues $\lambda_0=\pm1.5492i$, $\pm1.2247i$ and $\lambda_2=\pm2.3113i$, $\pm1.1322i$, respectively. In addition, there is a hyperbolic fixed point $(X_1,A_1)=(0.1976,0.2223)$ between them with eigenvalues $\lambda_1=\pm1.7778i$, ±1.1484. The fixed point (X_0,A_0) corresponds to a state of complete annihilation of the kink and antikink forms with the scalar field settling into the $\phi=-1$ stable vacuum solution. The fixed points (X_2,A_2) and (X_1,A_1) are localized solutions representing stable and unstable stationary bound-state solutions, respectively, that satisfy $\phi(x=\pm\infty,t)=-1$.

Figures 16 and 17 show contours or different level curves of the effective potential V_{eff} defined by (4.10). The contours were obtained by solving (4.10) as a quadratic equation for A:

$$A=\frac{F}{\omega_1^2}\pm\frac{1}{\omega_1^2}[F^2+\omega_1^2(V_{\text{eff}}-U)]^{1/2}\ , \tag{4.11}$$

and plotting the results for different values of V_{eff}. Note

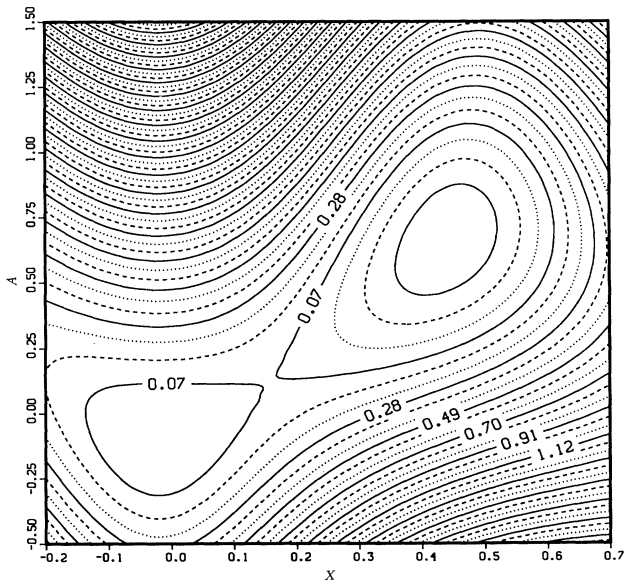

FIG. 17. Isolation of the immediate regions surrounding the three fixed points.

TABLE IV. Initial impact velocity intervals for the first five windows in the two-bounce kink-antikink interactions for the reduced system of equations.

m	v_1	v_2	Δv	Δv_n	β
1	0.199 765	0.215 490	0.015 725	1.0	
2	0.254 050	0.259 230	0.005 180	0.329 412	3.86
3	0.270 260	0.272 533	0.002 273	0.144 547	3.79
4	0.277 269	0.278 475	0.001 206	0.076 693	3.70
5	0.280 942	0.281 632	0.000 690	0.043 879	3.69

that because we are simulating the collision of widely separated kink and antikink, it is necessary that X be large and open channels of infinite extent are expected. The limit $X\to\infty$ implies that $F\to 0$ and $U\to 4\sqrt{2}/3=2M_0$. So we get from (4.11) that $A=\pm(1/\omega_1)(V_{\rm eff}-4\sqrt{2}/3)^{1/2}$, which sets a constraint on the effective potential, $V_{\rm eff}>4\sqrt{2}/3=2M_0$. For values of $V_{\rm eff}$ less than this, the potential represents a bounded or closed system. Figure 16 displays three level curves of the effective potential: closed with $V_{\rm eff}=M_0$, critically bounded with $V_{\rm eff}=2M_0$, and a wide channel with $V_{\rm eff}=3M_0$. Figure 17 is an isolation of the local regions surrounding the three critical points and clearly identifying the elliptic and hyperbolic points.

Hamilton's equations (4.9) are solved numerically using a fourth-order Runge-Kutta method. Care must be taken when solving these equations because as kink and antikink approach each other, $|X|$ goes to zero (in fact, Fig. 16 shows that X can become negative), and although the expressions (4.5) are well defined for $X=0$, they are composed of individual terms that become infinite, creating difficulties with our numerical solutions. This can be avoided by expanding (4.5) in powers of X for $|X|\ll 1$ to give, in terms of $\alpha=\sqrt{2}X$,

$$
\begin{aligned}
I &= M_0\left(1-\tfrac{2}{5}\alpha^2+\tfrac{2}{21}\alpha^4\right), \\
F &= \frac{\pi\sqrt{M_0}}{4\sqrt{2}}\left(9\alpha^2-15\alpha^4\right), \\
U &= \frac{4M_0}{5}\left(3\alpha^2-2\alpha^3+\tfrac{1}{7}\alpha^4\right),
\end{aligned}
\tag{4.12}
$$

and

$$
\begin{aligned}
I' &= \sqrt{2}M_0\left(-\tfrac{4}{5}\alpha+\tfrac{8}{21}\alpha^3\right), \\
F' &= \frac{\pi\sqrt{M_0}}{4}\left(18\alpha-60\alpha^3\right), \\
U' &= \frac{4M_0\sqrt{2}}{5}\left(6\alpha-6\alpha^2+\tfrac{4}{7}\alpha^3+\tfrac{10}{7}\alpha^4\right),
\end{aligned}
\tag{4.13}
$$

for a series accurate to fourth order in α. These equations are solved in place of the full unperturbed equations whenever $|X|$ becomes too small ($|X|\le 0.0005$). Using this procedure, the total energy given by the Hamiltonian (4.6) is conserved to better than one part in 10^7 in our simulations for the worst-case scenarios simulating erratic bion states with time steps set by $\Delta t=0.01$.

The initial conditions used in all our simulations were $X_0=7$, $A_0=\dot{A}_0=0$, and the velocity $\dot{X}_0\equiv -v_\infty$ is the free parameter. Note that because of the exponential dependence of U, F, and I on X, the large value of the initial data chosen for X_0 is effectively infinity with $I,F\approx 0$ and $U\approx 4\sqrt{2}/3$. Under these initial conditions the Hamiltonian (4.6) can be written as $H\approx M_0(\dot{X}^2+2)=2\sqrt{2}(v_\infty^2+2)/3$. Varying v_∞ gives us different potential contours. The condition $V_{\rm eff}>4\sqrt{2}/3$ necessary for extended channels to exist is equivalent to setting $|v_\infty|>0$. Also, the effect of increasing $|v_\infty|$ increases the value of H, which results in wider channels, as observed in Fig. 16.

Numerical simulations of the reduced system of equations (4.9) have shown a similar dependence on the impact velocity as the fully infinite-dimensional system (2.3).

TABLE V. Initial impact velocity intervals for the first five windows in the three-bounce kink-antikink interactions found near the first two-bounce windows. Results are for the reduced system of equations.

m	v_1	v_2	Δv	Δv_n	β
1	0.222 875 8	0.223 473 8	0.000 598 0		
2	0.218 006 2	0.218 391 2	0.000 385 0	1.0	
3	0.216 742 5	0.216 907 5	0.000 165 0	0.428 571 4	2.95
4	0.216 246 0	0.216 325 5	0.000 079 5	0.206 493 5	3.09
5	0.216 000 9	0.216 044 6	0.000 043 7	0.113 506 4	3.14

TABLE VI. Initial impact velocity intervals for the first five windows in the three-bounce kink-antikink interactions found near the second two-bounce window. Results are for the reduced system of equations.

m	v_1	v_2	Δv	Δv_n	β
1	0.260 927 1	0.261 087 7	0.000 160 6		
2	0.259 810 8	0.259 907 0	0.000 096 2	1.0	
3	0.259 525 3	0.259 565 8	0.000 040 5	0.420 997 9	3.01
4	0.259 415 9	0.259 435 5	0.000 019 6	0.203 742 2	3.11
5	0.259 363 0	0.259 373 6	0.000 010 6	0.110 187 1	3.18

In particular, we have observed analogous sequences of n-bounce windows which we have summarized in Table IV for the two-bounce windows and Tables V and VI for the three-bounce windows near the first and second two-bounce windows, respectively. A fractal structure such as that reported in Sec. II appears also in the reduced equations. This result is anticipated since the reduced equations model the shape-mode vibrations which were determined in Sec. III to be the source of the resonance windows. However, it can be seen that restriction to finite phase space substantially changes the quantitative parameters of the structure, including the window size and the fractal exponent β, which is more erratic and larger in the reduced phase-space case.

Examples of the two- and three-bounce solutions in this reduced model are presented in Figs. 18–21. Figures 18 and 19 show $\phi(x=0,t)$ defined in (4.2) for the first two two-bounce windows with $v_\infty=0.2$ and 0.255, respectively, while Figs. 20 and 21 display the first two three-bounce windows near the first two-bounce window for $v_\infty=0.183$ and 0.194, respectively. The resonance condition (3.6) between the period of collisions and the frequency of internal mode vibrations was tested for the first two-bounce window. A least-squares fit gave a straight line with slope 5.11, which models the numerical data very well and is also in excellent agreement with $2\pi/(\omega_1)=5.13$, which one expects from (3.6).

We present graphs of the separation distance $X(t)$ in Fig. 22 and the internal mode amplitudes $A(t)$ in Fig. 23 for the first three-bounce window with $v_\infty=0.183$. Figures 22 and 23 clearly show the three-bounce signature as $X\to 0$ and the internal mode amplitudes become strongest. In addition, the two-soliton solutions in the n-bounce windows are characterized by a linear growth in separation distance (solitons move away from each other with constant velocity) during which the internal mode excitations are simple periodic oscillations with frequency ω_1. This is predicted from Eqs. (4.9) by taking the limit $X\gg 1$ corresponding to a separated kink-antikink configuration to get $\ddot{X}\approx 0$ and $\ddot{A}\approx-\omega_1 A$ with the trivial solutions $X=\dot{X}_0 t+X_0$ and $A=A_0 e^{\pm i\omega_1 t}$. Another representation of the same case ($v_\infty=0.183$) is shown in Fig. 24 where we have plotted the phase-space trajectory (dotted line) in the X-A plane. Boundaries on the motion (solid line) are defined by the level curve for $V_{\text{eff}}=M_0(v_\infty^2+2)$.

Although the fractal resonance structure present in the full infinite-dimensional system is reproduced nicely by the reduced model, we point out that the reduced equations ignore energy radiated in the collision process. In addition to shifting the exact scaling of the solution, radiation dissipation is expected to contribute to the existence of long-lived bound states which occupy the complementary velocity space between reflection windows.

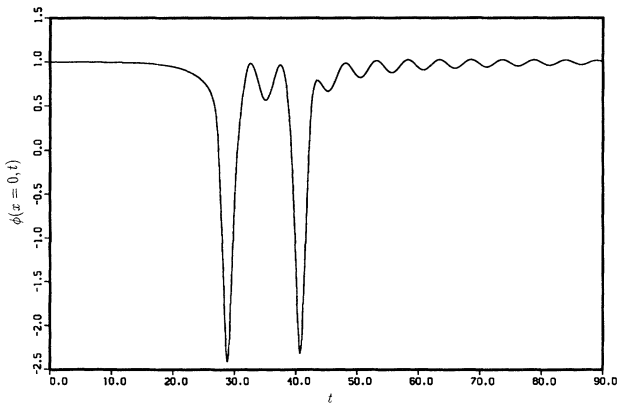

FIG. 18. Center-of-mass $\phi(x=0,t)$ evolution for the first two-bounce window with $v_\infty=0.2$ in the reduced system of equations.

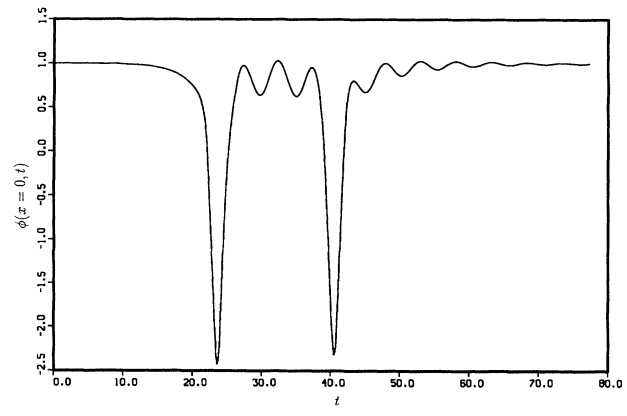

FIG. 19. Center-of-mass $\phi(x=0,t)$ evolution for the second two-bounce window with $v_\infty=0.255$ in the reduced system of equations.

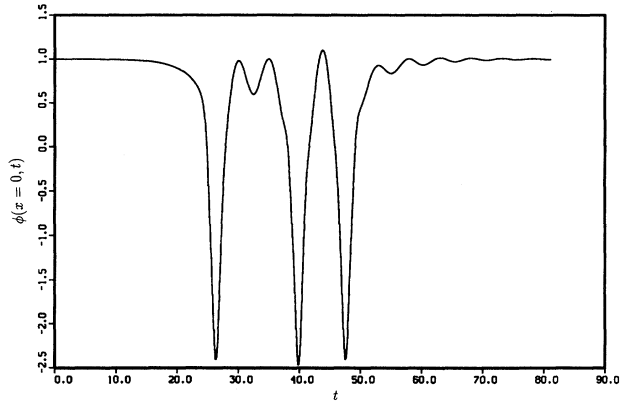

FIG. 20. Center-of-mass $\phi(x=0,t)$ evolution for the first three-bounce window near the first two-bounce window with $v_\infty=0.223$ in the reduced system of equations.

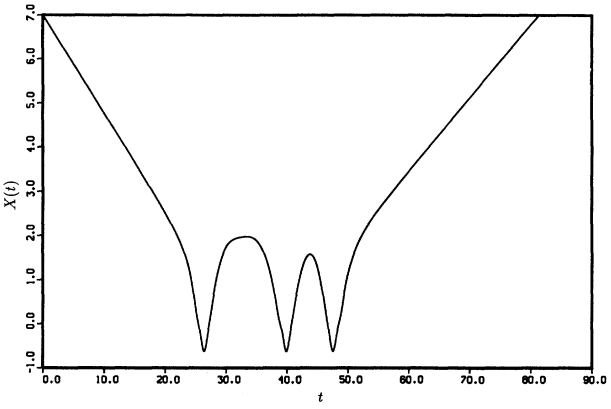

FIG. 22. Separation distance X vs time for the first three-bounce window ($v_\infty=0.223$) in the reduced system of equations.

Neglecting radiation in the reduced model should alter the complementary space in the fractal structure. In fact, we have not observed any long-lived bion states in our numerical work dealing with the reduced equations. Given enough time, all trajectories that we have simulated eventually escape through the open channel to infinity, forming a two-soliton solution.

We have investigated the nature of bion states existing in the reduced system in the endeavor to determine if the oscillatory behavior is chaotic. Because the bion state is bounded in phase space, some common techniques of analysis are directly applicable. In Fig. 25 we present a Poincaré section in the A-$\dot{A}$ plane for the case $v_\infty=0.02$. The Poincaré map is generated by plotting the points which cross the $X=0$ surface with positive momentum ($\dot{X}>0$). The solid line represents bounds on the potential in the Hamiltonian (4.6) obtained by setting $X=\dot{X}=0$ to get $\dot{A}=\pm(H-w_1^2A^2)^{1/2}$. Figure 25 shows that the trajectory wanders ergodically through the energy surface with no evidence of smooth invariant curves. The low value of v_∞ ($=0.02$) produces a very narrow channel in the contour of V_{eff} of infinite extent. Narrower channels reduce the liklihood that phase trajectories could escape to infinite separation distances. This effectively increases the bion lifetime.

We have also computed the maximum Lyapunov exponent for the bion state ($v_\infty=0.02$) by solving for deviations in two initially nearby trajectories [20]. This is accomplished by linearizing the autonomous differential equations (4.9), which we write schematically as

$$\frac{dy_i}{dt}=F_i,\quad i=1,4\ , \tag{4.14}$$

for a four-dimensional phase space. Linearizing about any reference orbit $y_i=y_{i0}+\delta y_i$ yields

$$\frac{d\delta y_i}{dt}=\sum_{j=1}^{4}\delta y_j J_i^j\ , \tag{4.15}$$

where $J_i^j=\partial F_i/\partial y_0|_{y=y_0}$ is the Jacobian matrix. Deviations between two trajectories are defined by $d(t)=[\sum_{i=1}^{4}\delta y_i^2(t)]^{1/2}$. To prevent computer overflow which can result if $d(t)$ increases exponentially, we use

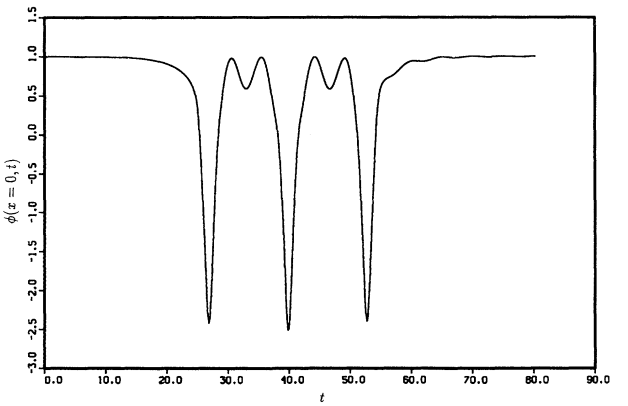

FIG. 21. Center-of-mass $\phi(x=0,t)$ evolution for the second three-bounce window near the first two-bounce window with $v_\infty=0.2182$ in the reduced system of equations.

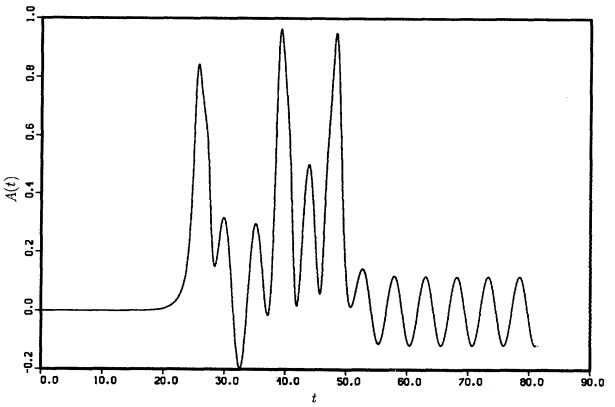

FIG. 23. Amplitude of internal mode vibrations, A, vs time for the first three-bounce window ($v_\infty=0.223$) in the reduced system of equations.

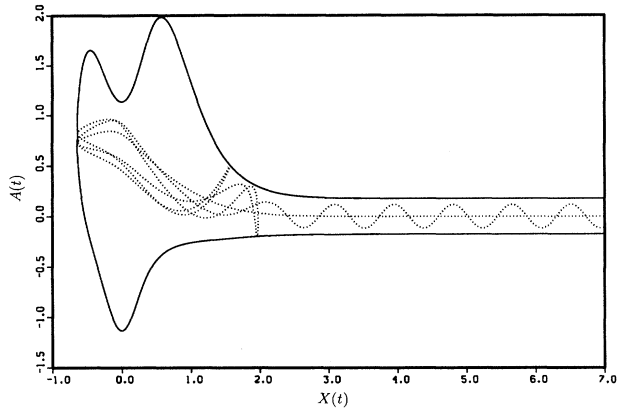

FIG. 24. Trajectory (dotted line) in the X-A phase plane for the first three-bounce window ($v_\infty = 0.223$) in the reduced system of equations. Boundaries on the motion (solid line) are defined by the appropriate level curve for $V_{\text{eff}} = M_0(v_\infty^2 + 2)$.

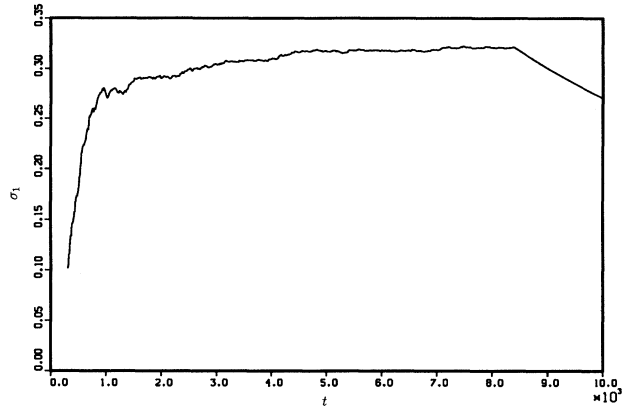

FIG. 26. Maximum Lyapunov exponent for $v_\infty = 0.02$ settles to a positive constant (≈ 0.32), demonstrating the chaotic nature of bion oscillations. The sharp decline in σ_1 starting at $t \sim 8300$ indicates that the bion state in the reduced system escaped through a channel to infinity in phase space and physically has broken up into a two-soliton state.

the scheme suggested by Benettin [21], which begins with the initial deviation $d(0)$ normalized to unity. The divergence d_j is computed over some interval τ using (4.15) and then renormalized back to unity to be used again as the initial deviation for the next interval of time. Using deviations computed in this fashion, the maximum Lyapunov exponent (σ_1) is defined by [20,21]

$$\sigma_1 = \lim_{N\to\infty} \frac{1}{N\tau} \sum_{j=1}^{N} \ln d_j \ . \tag{4.16}$$

We present a plot of σ_1 versus time for $v_\infty = 0.02$ in Fig. 26, which clearly shows that σ_1 approaches a well-defined positive constant ≈ 0.32 (before dropping sharply), signifying that nearby trajectories diverge exponentially. This value for σ_1 is in agreement with λ_1 found in Sec. II, supporting our claim that bion-state oscillations are chaotic. It is interesting to note that the point at which σ_1 begins to decrease sharply ($t \approx 8300$) occurs as the phase trajectory finds its way into the open channel and is forced by the potential walls to behave in a regular fashion (X increases linearly and A oscillates periodically with fixed frequency ω_1). As a result, nearby trajectories diverge linearly rather than exponentially. In other words, the bion state at $t \sim 8300$ has broken up to form an integrable two-soliton solution with the two solitons moving apart at constant velocity.

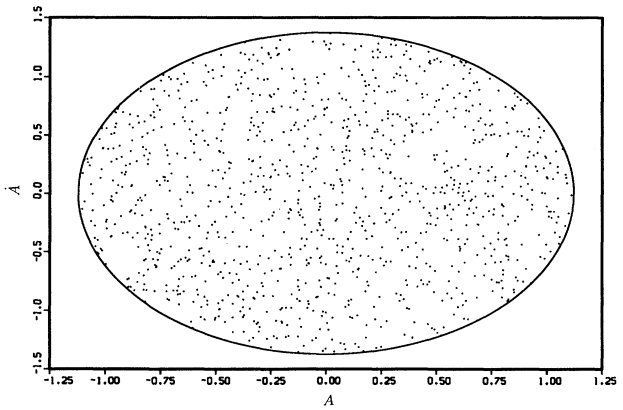

FIG. 25. Poincaré section in the A-$\dot{A}$ plane for a bion state with $v_\infty = 0.02$ in the reduced system of equations.

V. CONCLUSIONS

We have observed a remarkable fractal structure in the parameter space of impact velocity describing a competition between a bion state and a two-soliton solution which can result from kink-antikink collisions. The impact-parameter space is a complex self-similar fractal composed of sequences of different n-bounce reflection windows separated by regions of bion states. On a fractal set of values of the impact velocity, a kink-antikink collision forms a bound state. It has been demonstrated through perturbation theory that the fractal structure can be understood as a resonance condition associated with an energy exchange between the translational mode and the internal shape-mode oscillations. Chaotic behavior has been confirmed for the oscillating bion state by computing the maximum Lyapunov exponent.

The method of collective coordinates has proven to be a powerful method when applied to simplify the scalar field equation. Although one should not expect the reduced equations to exactly model the full infinite-dimensional system, we have demonstrated that a reduction of the exact system to one with just two degrees of freedom (modeling the translational and internal shape modes) reproduces remarkably well some of the behavior of the full dynamical system. In particular, we have observed sequences of n-bounce reflection windows forming a fractal structure similar to that found in the fully infinite-dimensional system. We have also verified the chaotic nature of the bion state in the reduced system by computing the maximum Lyapunov exponent and found it to be in agreement with that computed for the infinite-

dimensional case.

The main differences in the full and reduced system are attributed to neglecting the radiation dissipated during the collision process which contributes to the existence of long-lived bound states.

Chaotic behavior is now a well-studied phenomenon in bounded dynamical systems. Hamiltonian systems with an unbounded phase space (such as the one described in this paper) representing irregular scattering processes are known to exhibit chaotic motion with underlying mechanisms similar to those found in bounded systems [22]. Chaos, or the sensitive dependence on initial conditions, in these systems shows up as a Cantor set of singularities for which scattering is not defined (for example, initial conditions which lead to trapped states). Slight changes in the initial data may cause dramatic changes in the final states. In view of such systems, our results are not unexpected.

ACKNOWLEDGMENTS

We thank A. Wolf for sending us a copy of the program FET used to compute Lyapunov exponents from a time series and for making clear the significance of the various input parameters. S. O. was supported in part by CAPES (a Brazilian Education Council) and Universidade de Brasilia, Brazil. Computations reported here were carried out at the National Center for Super Computer Applications (University of Illinois) and at the UT-CHPC computational facility (University of Texas at Austin). This work was supported by NSF Grant No. PHY8806567.

---

*On leave from Departamento de Fisica, Universidade de Brasilia, 70.000 Brasilia, Brazil.

[1] P. Collins *et al., Particle Physics and Cosmology* (Wiley, New York, 1989), Chap. 17.
[2] C. T. Hill, D. N. Schramm, and J. Fry, Comments Nucl. Part. Phys. **19**, 25 (1989).
[3] A. Stebbins and M. S. Turner, Astrophys. J. Lett. **339**, L13 (1989).
[4] W. Press *et al.,* Astrophys. J. **347**, 590 (1989).
[5] L. Widrow, Phys. Rev. D **40**, 1002 (1989).
[6] E. Infeld and G. Rowlands, *Nonlinear Waves, Solitons and Chaos* (Cambridge University Press, Cambridge, England, 1990).
[7] F. Abdullaevv, Phys. Rep. **179**, 1 (1989).
[8] F. G. Bass *et al.,* Phys. Rep. **157**, 63 (1988).
[9] Y. Kivshar and B. Malomed, Rev. Mod. Phys. **61**, 763 (1989).
[10] V. Makhankov, Phys. Rep. **35**, 1 (1978).
[11] P. Drazin and R. Johnson, *Solitons: An Introduction* (Cambridge University Press, Cambridge, England, 1989).
[12] T. Sugiyama, Prog. Theor. Phys. **61**, 1550 (1979).
[13] D. Campbell *et al.,* Physica D **9**, 1 (1983).
[14] V. Silveira, Phys. Rev. D **38**, 3823 (1988).
[15] T. Belova and A. Kudryavtsev, Physica D **32**, 18 (1988).
[16] R. W. Hornbeck, *Numerical Methods* (Prentice-Hall, Englewood Cliffs, NJ, 1975).
[17] F. Takens, in *Dynamical Systems and Turbulence, Warwick 1980,* Proceedings of a Symposium, Coventry, England, edited by D. A. Rand and L.-S. Young, Lecture Notes in Mathematics, Vol. 898 (Springer, New York, 1981).
[18] A. Wolf *et al.,* Physica D **16**, 285 (1986).
[19] G. D. Billing, Comput. Phys. Rep. **12**, 383 (1990).
[20] M. Tabor, *Chaos and Integrability in Nonlinear Dynamics: An Introduction* (Wiley, New York, 1989).
[21] G. L. Benettin, Phys. Rev. A **14**, 2338 (1976).
[22] B. Eckhardt, Physica D **33**, 89 (1988).